CHAPTER FIFTEEN

Finite Volume Methods via Finite Element Methods

15.1 GENERAL

The finite volume methods (FVM) via FDM discussed in Chapter 7 may also be formulated using finite element methods (FEM). Schneider and Raw [1987], Masson, Saabas, and Baliga [1994], and Darbandi and Schneider [1999], among many others, contributed to the earlier and recent developments of FVM via FEM.

The FVM equations via finite elements are the same as those given in (7.1.4) for the case of the Navier-Stokes system of equations using finite differences,

$$\sum_{CV}\left(\frac{\Delta \mathbf{U}}{\Delta t}-\mathbf{B}\right)\Delta\Omega+\sum_{CS}(\mathbf{F}_i+\mathbf{G}_i)n_i\Delta\Gamma=0 \tag{15.1.1a}$$

or

$$\sum_{CV}(\Delta\mathbf{U}-\Delta t\mathbf{B})\Delta\Omega+\Delta t\sum_{CS}(\mathbf{F}_i+\mathbf{G}_i)n_i\Delta\Gamma=0 \tag{15.1.1b}$$

It is seen that quantities to be evaluated are involved in control volumes $\Delta\Omega$ and control surfaces $\Delta\Gamma$. We shall demonstrate how they are evaluated using finite elements in this chapter.

Consider the two-dimensional geometry as shown in Figure 15.1.1a. Note that global node 1 is surrounded by five elements, with each element divided into quadrilateral isoparametric elements (Figure 15.1.1b). A quadrant of each element is connected to node 1, forming five subcontrol volumes (CV1-A, CV1-B, CV1-C, CV1-D, and CV1-E). Each subcontrol volume has two control surfaces with outward normal directions with angles θ measured counterclockwise from the global reference cartesian x-coordinate.

It is reasonable to approximate $\Delta\mathbf{U}$ in control volumes with quadratic trial functions whereas the fluxes ($\mathbf{F}_i$ and $\mathbf{G}_i$) in control surfaces may be approximated by linear trial functions. Fluxes evaluated for all control volumes along the control surfaces plus the control volume quantities ($\Delta\mathbf{U}$ and $\mathbf{B}$) are to be assembled into each global node (control volume center), resulting in simultaneous algebraic equations for the entire system.

Note that the fluxes along the control surfaces are equal with opposite signs between neighboring control surfaces. This process renders all fluxes completely conserved – a distinctive advantage of FVM.

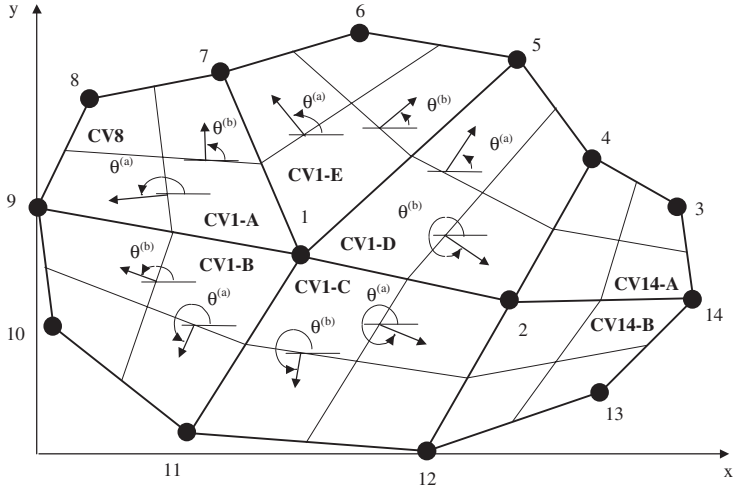

(a)

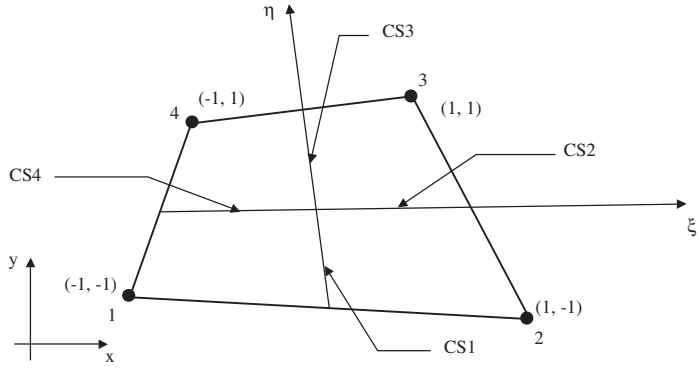

(b)

Figure 15.1.1 Unstructured grids for finite elements – node-centered control volume. **(a)** Subcontrol volumes CV1-A, B, C, D, E surrounding Node 1 with components of vectors normal to all control surfaces, subcontrol volume for node 8 (CV 8), subcontrol volumes for node 14 (CV14-A, B). **(b)** Control surfaces CS1, 2, 3, 4 with integration points along $\eta = 0$, $\xi = 0$ axes at centers of control surfaces in isoparametric element with corner nodes 1, 2, 3, 4.

Implementation of the finite element approximations toward FVM for two- and three-dimensional problems will be presented in the following subsections.

15.2 FORMULATIONS OF FINITE VOLUME EQUATIONS

15.2.1 BURGERS' EQUATIONS

To compare the formulation and solution procedure of FVM with FEM, let us consider the two-dimensional Burgers' equation in the form

$$\frac{\partial \mathbf{U}}{\partial t} + u\frac{\partial \mathbf{U}}{\partial x} + \mathrm{v}\frac{\partial \mathbf{U}}{\partial y} - \nu\left(\frac{\partial^2 \mathbf{U}}{\partial x^2} + \frac{\partial^2 \mathbf{U}}{\partial y^2}\right) - \mathbf{F} = 0 \tag{15.2.1}$$

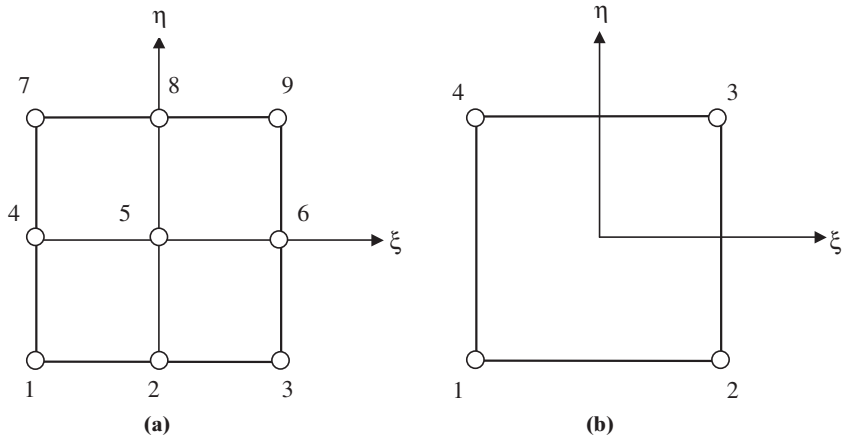

Figure 15.2.1 Isoparametric elements. **(a)** Quadratic approximation for control volumes. **(b)** Linear approximation for control surface.

where

$$\mathbf{U} = \begin{bmatrix} u \\ \mathrm{v} \end{bmatrix}, \qquad \mathbf{F} = \begin{bmatrix} f_x \\ f_y \end{bmatrix}$$

$$f_x = -\frac{1}{(1+t)^2} + \frac{x^2 + 2xy}{(1+t)} + 3x^3y^2 - 2\nu y$$

$$f_y = -\frac{1}{(1+t)^2} + \frac{y^2 + 2xy}{(1+t)} + 3y^3x^2 - 2\nu x$$

with the exact solution

$$u = \frac{1}{1+t} + x^2 y, \qquad \mathrm{v} = \frac{1}{1+t} + xy^2$$

To illustrate the implementation of both the Dirichlet and Neumann boundary conditions on inclined surfaces, we consider the discretized geometries as shown in Figure 15.2.1 on which basic FVM equations will be written in terms of isoparametric finite elements.

Finite volume equations may be constructed within the framework of a two-step Taylor-Galerkin formulation. Toward this end, we begin with

$$\mathbf{U}^{n+1} = \mathbf{U}^n + \Delta t \frac{\partial \mathbf{U}^n}{\partial t} + O(\Delta t^2)$$

This may be split into two steps:

Step 1

$$\mathbf{U}^{n+\frac{1}{2}} = \mathbf{U}^n + \frac{\Delta t}{2} \frac{\partial \mathbf{U}^n}{\partial t} \tag{15.2.2a}$$

Step 2

$$\mathbf{U}^{n+1} = \mathbf{U}^n + \Delta t \frac{\partial \mathbf{U}^{n+\frac{1}{2}}}{\partial t} \tag{15.2.2b}$$

with $\partial \mathbf{U}/\partial t$ being determined from (15.2.1):

$$\frac{\partial \mathbf{U}}{\partial t} = -u\frac{\partial \mathbf{U}}{\partial x} - \mathrm{v}\frac{\partial \mathbf{U}}{\partial y} + \nu\left(\frac{\partial^2 \mathbf{U}}{\partial x^2} + \frac{\partial^2 \mathbf{U}}{\partial y^2}\right) + \mathbf{F} \tag{15.2.3}$$

Substituting (15.2.3) into step 1 (15.2.2a) gives

$$\mathbf{U}^{n+\frac{1}{2}} = \mathbf{U}^n - \frac{\Delta t}{2}\left(u\frac{\partial \mathbf{U}^n}{\partial x} + \mathrm{v}\frac{\partial \mathbf{U}^n}{\partial y}\right) + \frac{\Delta t}{2}\nu\left(\frac{\partial^2 \mathbf{U}^n}{\partial x^2} + \frac{\partial^2 \mathbf{U}^n}{\partial y^2}\right) + \frac{\Delta t}{2}\mathbf{F}^n \tag{15.2.4}$$

Finite volume formulation using a unit test function becomes

$$\begin{aligned}\int_\Omega \mathbf{U}^{n+\frac{1}{2}} d\Omega = \int_\Omega \mathbf{U}^n d\Omega - \frac{\Delta t}{2}\int_\Omega \left(u\frac{\partial \mathbf{U}^n}{\partial x} + \mathrm{v}\frac{\partial \mathbf{U}^n}{\partial y}\right) d\Omega \\ + \frac{\Delta t}{2}\nu\int_\Omega \left(\frac{\partial^2 \mathbf{U}^n}{\partial x^2} + \frac{\partial^2 \mathbf{U}^n}{\partial y^2}\right) d\Omega + \frac{\Delta t}{2}\int_\Omega \mathbf{F}^n d\Omega\end{aligned} \tag{15.2.5}$$

Integrating by parts, we have

$$\begin{aligned}\int_\Omega \mathbf{U}^{n+\frac{1}{2}} d\Omega = \int_\Omega \mathbf{U}^n d\Omega - \frac{\Delta t}{2}\int_\Omega \left(u^n\frac{\partial \mathbf{U}^n}{\partial x} + \mathrm{v}^n\frac{\partial \mathbf{U}^n}{\partial y}\right) d\Omega \\ + \frac{\Delta t}{2}\nu\int_\Gamma \left(\frac{\partial \mathbf{U}^n}{\partial x}n_1 + \frac{\partial \mathbf{U}^n}{\partial y}n_2\right) d\Gamma + \frac{\Delta t}{2}\int_\Omega \mathbf{F}^n d\Omega\end{aligned} \tag{15.2.6}$$

Rewriting the integral as summations,

$$\begin{aligned}\sum_{CV} \mathbf{U}^{n+\frac{1}{2}}\Delta\Omega = \sum_{CV}\left[\mathbf{U}^n - \frac{\Delta t}{2}\left(u^n\frac{\partial \mathbf{U}^n}{\partial x} + \mathrm{v}^n\frac{\partial \mathbf{U}^n}{\partial y}\right) + \frac{\Delta t}{2}\mathbf{F}^n\right]\Delta\Omega \\ + \frac{\Delta t}{2}\nu\sum_{CS}\left(\frac{\partial \mathbf{U}^n}{\partial x}n_1 + \frac{\partial \mathbf{U}^n}{\partial y}n_2\right)\Delta\Gamma\end{aligned} \tag{15.2.7}$$

Similarly for step 2 (15.2.2b), we have

$$\begin{aligned}\sum_{CV} \mathbf{U}^{n+1}\Delta\Omega = \sum_{CV}\left[\mathbf{U}^n - \frac{\Delta t}{2}\left(u^{n+\frac{1}{2}}\frac{\partial \mathbf{U}^{n+\frac{1}{2}}}{\partial x} + \mathrm{v}^{n+\frac{1}{2}}\frac{\partial \mathbf{U}^{n+\frac{1}{2}}}{\partial y}\right) + \frac{\Delta t}{2}\mathbf{F}^{n+\frac{1}{2}}\right]\Delta\Omega \\ + \frac{\Delta t}{2}\nu\sum_{CS}\left(\frac{\partial \mathbf{U}^{n+\frac{1}{2}}}{\partial x}n_1 + \frac{\partial \mathbf{U}^{n+\frac{1}{2}}}{\partial y}n_2\right)\Delta\Gamma\end{aligned} \tag{15.2.8}$$

Note that in these two-step solutions, (15.2.7) and (15.2.8), derivatives of $\mathbf{U}(d\mathbf{U}/dx$ and $d\mathbf{U}/dy)$ are involved within the control volumes and along the control surfaces. Quadratic and linear isoparametric finite element approximations are used, respectively, for control volumes and control surfaces, as shown in Figure 15.2.2. Derivatives of $\mathbf{U}$ involve the transformation between the isoparametric and cartesian coordinates as shown in Chapter 9. Derivatives involved in control volumes and control surfaces are carried out as follows:

For Control Volumes (quadratic approximation)

$$\frac{\partial \mathbf{U}}{\partial x_i} = \sum_{N=1}^{9} \left(\frac{\partial \Phi_N^{(e)}}{\partial x_i} \mathbf{U}_N \right)_{\xi=0,\,\eta=0}$$
$$= \begin{bmatrix} \frac{1}{4|J|}[(\mathbf{U}_2 - \mathbf{U}_8)(y_6 - y_4) - (\mathbf{U}_6 - \mathbf{U}_4)(y_2 - y_8)] \\ \frac{1}{4|J|}[(\mathbf{U}_2 - \mathbf{U}_8)(x_6 - x_4) - (\mathbf{U}_6 - \mathbf{U}_4)(x_2 - x_8)] \end{bmatrix} \tag{15.2.9}$$

with

$$|J| = \frac{1}{4}[(x_2 - x_8)(y_6 - y_4) - (x_6 - x_4)(y_2 - y_8)] \tag{15.2.10}$$

For Control Surfaces (linear approximation)

$$\sum_{CS} \left(\frac{\partial \mathbf{U}}{\partial x} n_1 + \frac{\partial \mathbf{U}}{\partial y} n_2 \right) \Delta\Gamma = \sum_{CS2,3} \left(\frac{\partial \mathbf{U}}{\partial x} n_1 + \frac{\partial \mathbf{U}}{\partial y} n_2 \right) \Delta\Gamma + \sum_{CS4,3} \left(\frac{\partial \mathbf{U}}{\partial x} n_1 + \frac{\partial \mathbf{U}}{\partial y} n_2 \right) \Delta\Gamma$$
$$+ \sum_{CS1,4} \left(\frac{\partial \mathbf{U}}{\partial x} n_1 + \frac{\partial \mathbf{U}}{\partial y} n_2 \right) \Delta\Gamma + \sum_{CS1,2} \left(\frac{\partial \mathbf{U}}{\partial x} n_1 + \frac{\partial \mathbf{U}}{\partial y} n_2 \right) \Delta\Gamma \tag{15.2.11}$$

with

$$\frac{\partial \mathbf{U}}{\partial x} = \frac{1}{|J|} \left(\frac{\partial \mathbf{U}}{\partial \xi} \frac{\partial y}{\partial \eta} - \frac{\partial \mathbf{U}}{\partial \eta} \frac{\partial y}{\partial \xi} \right) \tag{15.2.12a}$$

$$\frac{\partial \mathbf{U}}{\partial y} = \frac{1}{|J|} \left(-\frac{\partial \mathbf{U}}{\partial \xi} \frac{\partial x}{\partial \eta} + \frac{\partial \mathbf{U}}{\partial \eta} \frac{\partial x}{\partial \xi} \right) \tag{15.2.12b}$$

$$|J| = \frac{\partial x}{\partial \xi} \frac{\partial y}{\partial \eta} - \frac{\partial y}{\partial \xi} \frac{\partial x}{\partial \eta} \tag{15.2.13}$$

The above quantities are to be evaluated for each of the subcontrol volumes A, B, C, and D, corresponding to control surfaces (see Figure 15.2.2):

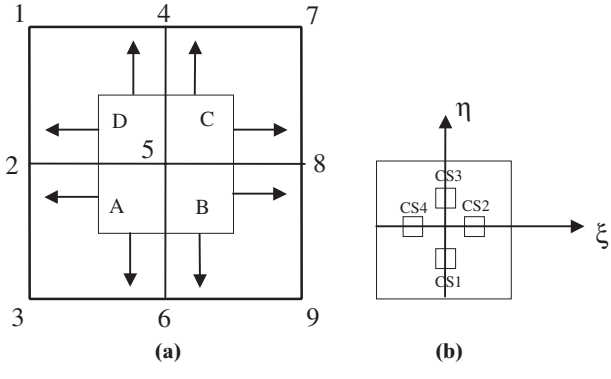

Figure 15.2.2 Control surfaces and their contributions to control volume at node 5 consisting of subcontrol volumes A, B, C, and D. **(a)** Control surfaces contributing to control volume. **(b)** Control surfaces evaluated at midpoints for each subcontrol volume.

CS2 and CS3 for A
CS3 and CS4 for B
CS4 and CS1 for C
CS1 and CS2 for D

Subcontrol Volume A

Control Surface CS2 ($\xi = 1/2, \eta = 0$)

$$\frac{\partial \mathbf{U}}{\partial \xi} = \frac{1}{4}(-\mathbf{U}_3 + \mathbf{U}_6 + \mathbf{U}_5 - \mathbf{U}_2)$$

$$\frac{\partial \mathbf{U}}{\partial \eta} = \frac{1}{8}(-\mathbf{U}_3 - 3\mathbf{U}_6 + 3\mathbf{U}_5 + \mathbf{U}_2)$$

Control Surface CS3 ($\xi = 0, \eta = 1/2$)

$$\frac{\partial \mathbf{U}}{\partial \xi} = \frac{1}{8}(-\mathbf{U}_3 + \mathbf{U}_6 + 3\mathbf{U}_5 - 3\mathbf{U}_2)$$

$$\frac{\partial \mathbf{U}}{\partial \eta} = \frac{1}{4}(-\mathbf{U}_3 - \mathbf{U}_6 + \mathbf{U}_5 + \mathbf{U}_2)$$

Sum the Control Surfaces CS2 and CS3

$$\sum_{CS2,3}^{A} \left(\frac{\partial \mathbf{U}}{\partial x} n_1 + \frac{\partial \mathbf{U}}{\partial y} n_2\right) \Delta\Gamma = \left(\frac{\partial \mathbf{U}}{\partial x} \cos\theta_2 + \frac{\partial \mathbf{U}}{\partial y} \sin\theta_2\right) \Delta\Gamma + \left(\frac{\partial \mathbf{U}}{\partial x} \cos\theta_3 + \frac{\partial \mathbf{U}}{\partial y} \sin\theta_3\right) \Delta\Gamma$$

with

$$|J| = \frac{1}{32}[(-x_3 + x_6 + 3x_5 - 3x_2)(-y_3 - y_6 + y_5 + y_2) - (-y_3 + y_6 + 3y_5 - 3y_2)(-x_3 - x_6 + x_5 + x_2)]$$

Subcontrol Volume B

Control Surface CS3 ($\xi = 0, \eta = 1/2$)

$$\frac{\partial \mathbf{U}}{\partial \xi} = \frac{1}{8}(-\mathbf{U}_6 + \mathbf{U}_9 + 3\mathbf{U}_8 - 3\mathbf{U}_5)$$

$$\frac{\partial \mathbf{U}}{\partial \eta} = \frac{1}{4}(-\mathbf{U}_6 - \mathbf{U}_9 + \mathbf{U}_8 + \mathbf{U}_5)$$

Control Surface CS4 ($\xi = -1/2, \eta = 0$)

$$\frac{\partial \mathbf{U}}{\partial \xi} = \frac{1}{4}(-\mathbf{U}_6 + \mathbf{U}_9 + \mathbf{U}_8 - \mathbf{U}_5)$$

$$\frac{\partial \mathbf{U}}{\partial \eta} = \frac{1}{8}(-\mathbf{U}_6 - 3\mathbf{U}_9 + 3\mathbf{U}_8 + \mathbf{U}_5)$$

Subcontrol Volume C

Control Surface CS4 ($\xi = -1/2, \eta = 0$)

$$\frac{\partial \mathbf{U}}{\partial \xi} = \frac{1}{4}(-\mathbf{U}_5 + \mathbf{U}_8 + \mathbf{U}_7 - \mathbf{U}_4)$$

$$\frac{\partial \mathbf{U}}{\partial \eta} = \frac{1}{8}(-3\mathbf{U}_5 - \mathbf{U}_8 + \mathbf{U}_7 + 3\mathbf{U}_4)$$

Control Surface CS1 ($\xi = 0, \eta = -1/2$)

$$\frac{\partial \mathbf{U}}{\partial \xi} = \frac{1}{8}(-3\mathbf{U}_5 + 3\mathbf{U}_8 + \mathbf{U}_7 - \mathbf{U}_4)$$

$$\frac{\partial \mathbf{U}}{\partial \eta} = \frac{1}{4}(-\mathbf{U}_5 - \mathbf{U}_8 + \mathbf{U}_7 + \mathbf{U}_4)$$

Subcontrol Volume D

Control Surface CS1 ($\xi = 0, \eta = -1/2$)

$$\frac{\partial \mathbf{U}}{\partial \xi} = \frac{1}{8}(-3\mathbf{U}_2 + 3\mathbf{U}_5 + \mathbf{U}_4 - \mathbf{U}_1)$$

$$\frac{\partial \mathbf{U}}{\partial \eta} = \frac{1}{4}(-\mathbf{U}_2 - \mathbf{U}_5 + \mathbf{U}_4 + \mathbf{U}_1)$$

Control Surface CS2 ($\xi = 1/2, \eta = 0$)

$$\frac{\partial \mathbf{U}}{\partial \xi} = \frac{1}{4}(-\mathbf{U}_2 + \mathbf{U}_5 + \mathbf{U}_4 - \mathbf{U}_1)$$

$$\frac{\partial \mathbf{U}}{\partial \eta} = \frac{1}{8}(-\mathbf{U}_2 - 3\mathbf{U}_5 + 3\mathbf{U}_4 + \mathbf{U}_1)$$

Assembly of the entire system is achieved by collecting contributions to an element from surrounding nodes in the first step and contributions to a node from surrounding elements in the second step, as shown in Figure 15.2.3.

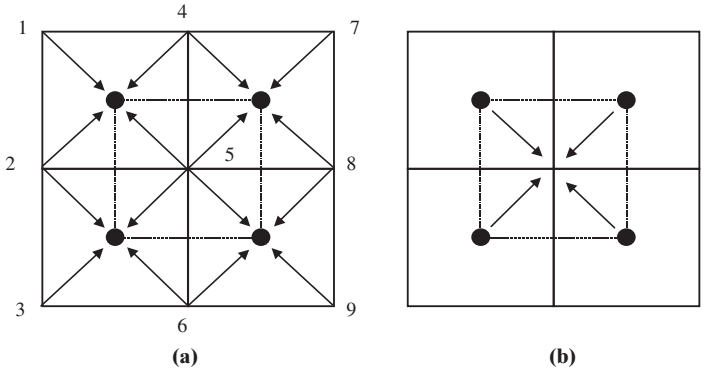

Figure 15.2.3 Contributions to an element from surrounding nodes and to a node from surrounding elements. **(a)** First step, contributions to an element from surrounding nodes. **(b)** Second step, contributions to a node from surrounding elements.

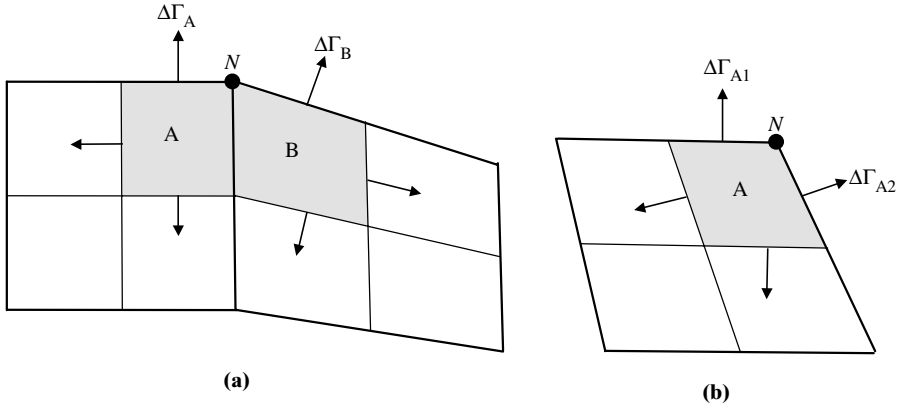

Figure 15.2.4 Treatment of Neumann boundary conditions. **(a)** Neumann boundary condition given at N joined by two inclined surfaces. **(b)** Neumann boundary condition given at corner node N.

Implementation of Neumann boundary conditions at the node with elements of inclined surfaces can be carried out easily. Consider the Neumann node N with two elements connected as shown in Figure 15.2.4a. The control surface equations for the Neumann node N become

$$\sum_{CS}\left(\frac{\partial \mathbf{U}}{\partial x}n_1+\frac{\partial \mathbf{U}}{\partial y}n_2\right)\Delta\Gamma=\sum_{CS3.2}^{A}\left(\frac{\partial \mathbf{U}}{\partial x}n_1+\frac{\partial \mathbf{U}}{\partial y}n_2\right)\Delta\Gamma+\sum_{CS4,3}^{B}\left(\frac{\partial \mathbf{U}}{\partial x}n_1+\frac{\partial \mathbf{U}}{\partial y}n_2\right)\Delta\Gamma$$
$$+\left(\frac{\partial \mathbf{U}}{\partial x}n_1+\frac{\partial \mathbf{U}}{\partial y}n_2\right)_A\Delta\Gamma_A+\left(\frac{\partial \mathbf{U}}{\partial x}n_1+\frac{\partial \mathbf{U}}{\partial y}n_2\right)_B\Delta\Gamma_B \tag{15.2.14}$$

The Neumann boundary conditions given at a corner with only one element (Figure 15.2.4b) can be implemented as

$$\sum_{CS}\left(\frac{\partial \mathbf{U}}{\partial x}n_1+\frac{\partial \mathbf{U}}{\partial y}n_2\right)\Delta\Gamma=\sum_{CS3.2}^{A}\left(\frac{\partial \mathbf{U}}{\partial x}n_1+\frac{\partial \mathbf{U}}{\partial y}n_2\right)\Delta\Gamma+\left(\frac{\partial \mathbf{U}}{\partial x}n_1+\frac{\partial \mathbf{U}}{\partial y}n_2\right)\Delta\Gamma_{A1}$$
$$+\left(\frac{\partial \mathbf{U}}{\partial x}n_1+\frac{\partial \mathbf{U}}{\partial y}n_2\right)\Delta\Gamma_{A2} \tag{15.2.15}$$

The source term $\mathbf{F}$ as given in (15.2.2a,b) can be computed at each control point using the control volume (area $\Delta\Omega$) with coordinates x and y corresponding to the control point.

All control volume and control surface equations for the two steps given by (15.2.7) and (15.2.8) are collected and assembled at each nodal control point, resulting in the global algebraic equations.

Generalized Petrov-Galerkin with PISO

Computational schemes as discussed in Chapter 12 may be used for the finite volume equations with integrations performed in the control volumes and control surfaces. An alternative technique is to use the PISO concept (Section 5.3.2), which is particularly

conducive to FVM formulation. In this approach, the predictor corrector steps are constructed as follows.

Step 1. Predictor. Integrating the momentum equations and writing them in control volumes and control surfaces,

$$\sum_{CV} \rho \left(\mathrm{v}_j^* - \mathrm{v}_j^n\right) \frac{\Delta\Omega}{\Delta t} = -\sum_{CS} \rho \left(\bar{\mathrm{v}}_i \mathrm{v}_j - \mu \mathrm{v}_{j,i} + p\delta_{ij}\right) n_i \Delta\Gamma \tag{15.2.16}$$

with

$\bar{\mathrm{v}}_i$ = the old time step value

$p = \Phi_N p_N$

$$\mathrm{v}_j = \begin{cases} W_N \mathrm{v}_{Nj} & \text{in convective term} \\ \Phi_N \mathrm{v}_{Nj} & \text{otherwise} \end{cases}$$

$W_N = \Phi_N + \Psi_N = \Phi_N + \beta g_k \Phi_{N,k}$

We may recast (15.2.16) in the form

$$K_N \mathrm{v}_{Nj}^* = R_j \tag{15.2.17}$$

$$K_N = \sum_{CV} \rho \frac{\Delta\Omega}{\Delta t} \Phi_N + \sum_{CS} \left(\rho \mathrm{v}_i^* W_N - \mu \Phi_{N,i}\right) n_i$$

$$R_j = \sum_{CV} \rho \frac{\Delta\Omega}{\Delta t} \mathrm{v}_{Nj}^* \Phi_N - \sum_{CS} \Phi_N n_j p_N$$

Here we solve v_{Nj}^* implicitly:

Step 2. (Corrector I). The momentum control volume and the control surface equations are corrected as

$$\sum_{CV} \rho \mathrm{v}_j^{**} \frac{\Delta\Omega}{\Delta t} = -\sum_{CS} \left(\rho \mathrm{v}_i^* \mathrm{v}_j^* - \mu \mathrm{v}_{i,j}^* + p\delta_{ij}\right) n_i \Delta\Gamma + \sum_{CV} \rho \mathrm{v}_j^n \frac{\Delta\Omega}{\Delta t} \tag{15.2.18}$$

To obtain the pressure correction equation, we differentiate spatially the momentum equation and integrate over the control volume in which we apply $\mathrm{v}_{i,j}^{**} = 0$. The resulting control surface equations become

$$\sum_{CS} p_{,i}^* n_i \Delta\Gamma = -\sum_{CS} \left(\rho \mathrm{v}_j^n n_j \frac{\Delta\Gamma}{\Delta t} - \rho \mathrm{v}_{i,j}^* \mathrm{v}_j^* + \rho \mathrm{v}_{j,i}^* \mathrm{v}_j^*\right) n_i \Delta\Gamma \tag{15.2.19}$$

where $\mathrm{v}_{j,ji}^* = 0$ with linear variation of Φ_α. In this step we compute p^* from (15.2.19) and v_j^{**} from (15.2.18) explicitly.

Step 3. (Corrector II). This is exactly the same as step 2 with (*) replaced by (**) and (**) replaced by (***). We solve for pressure p^{**} using

$$\sum_{CS} \Phi_{N,i} n_i \Delta\Gamma p_N^{**} = -\sum_{CS} \left(\rho \mathrm{v}_i^n n_i \frac{\Delta\Gamma}{\Delta t} - \rho \mathrm{v}_{i,j}^{**} \mathrm{v}_j^{**} + \rho \mathrm{v}_{j,i}^{**} \mathrm{v}_j^{**}\right) n_i \Delta\Gamma \tag{15.2.20}$$

and solve for velocity v_j^{***} explicitly using

$$\sum_{CV} \rho v_j^{***} \frac{\Delta\Omega}{\Delta t} = -\sum_{CS} (\rho v_i^{**} v_j^{**} - \mu v_{j,i}^{**} + p^{**}\delta_{ij}) n_i \Delta\Gamma + \sum_{CV} \rho v_j^n \frac{\Delta\Omega}{\Delta t} \tag{15.2.21}$$

The three steps are to be repeated until convergence is obtained.

15.2.2 INCOMPRESSIBLE AND COMPRESSIBLE FLOWS

(1) FVM with Two-step GTG Scheme

For the Burgers' equations considered in the previous sections, we evaluated derivatives along the control surfaces. If the Navier-Stokes system of equations is solved from the FVM equations of the type given by (15.1.1b), then we must evaluate the convection and diffusion fluxes ($\mathbf{F}_i$ and $\mathbf{G}_i$) directly along the boundary surfaces.

The FEM approximations for $\mathbf{U}$, $\mathbf{F}_i$, and $\mathbf{G}_i$ are given by

$$\begin{aligned} \Delta\mathbf{U} &= \Phi_N^{(e)} \Delta\mathbf{U}_N \\ \Delta\mathbf{F}_i &= \Phi_N^{(e)} \Delta\mathbf{F}_{Ni} \\ \Delta\mathbf{G}_i &= \Phi_N^{(e)} \Delta\mathbf{G}_{Ni} \end{aligned} \tag{15.2.22}$$

The two-step GTG scheme is the same as in (15.2.3):

Step 1

$$\sum_{CV} \mathbf{U}^{n+\frac{1}{2}} \Delta\Omega = \sum_{CV} (\mathbf{U}^n + \mathbf{B}^n) \Delta\Omega - \frac{\Delta t}{2} \sum_{CS} (\mathbf{F}_i^n + \mathbf{G}_i^n) n_i \Delta\Gamma \tag{15.2.23}$$

Step 2

$$\sum_{CV} \mathbf{U}^{n+1} \Delta\Omega = \sum_{CV} (\mathbf{U}^n + \mathbf{B}^n) \Delta\Omega - \frac{\Delta t}{2} \sum_{CS} (\mathbf{F}_i^{n+\frac{1}{2}} + \mathbf{G}_i^{n+\frac{1}{2}}) n_i \Delta\Gamma \tag{15.2.24}$$

The evaluation of $\mathbf{F}_i$, and $\mathbf{G}_i$ is carried out along the control surfaces, using (15.2.23 and 15.2.24) at the midpoints similarly as in the case of Burgers' equations presented in Section (15.2.1).

(2) FVM with PISO Approach

The FVM via FEM PISO approach can be extended to compressible flows similarly as in incompressible flows. This begins with integrating the momentum equations and writing them in control volumes and control surfaces,

$$\sum_{CV} \rho^n (v_j^* - v_j^n) \frac{\Delta\Omega}{\Delta t} = -\sum_{CS} [\rho^n \overline{v}_i v_j - \mu(v_{i,j} - v_{j,j}) + p\delta_{ij}] n_i \Delta\Gamma \tag{15.2.25}$$

The rest of the formulation follows the steps given in Section 6.3.4 by converting them into control volumes and control surfaces as shown in Section 15.2.2 for incompressible flows.

(3) FVM with Upwind Finite Elements

$$\frac{\partial \mathbf{U}}{\partial t}+\frac{\partial \mathbf{F}_i}{\partial x_i}+\frac{\partial \mathbf{G}_i}{\partial x_i}=0$$

$$\int_\Omega \frac{\partial \mathbf{U}}{\partial t}d\Omega+\int_\Omega\left(\frac{\partial \mathbf{F}_i}{\partial x_i}+\frac{\partial \mathbf{G}_i}{\partial x_i}\right)d\Omega=\int_\Omega \frac{\partial \mathbf{U}}{\partial t}d\Omega+\int_\Gamma(\mathbf{F}_i+\mathbf{G}_i)n_i d\Gamma=0 \tag{15.2.26}$$

(a) Inviscid Algorithm. Consider a typical flux change on the side r, s,

$$\Delta\mathbf{F}_i=\mathbf{F}_{ir}-\mathbf{F}_{is}=\mathbf{a}_i\Delta\mathbf{U}=\mathbf{a}_i(\mathbf{U}_r-\mathbf{U}_s)\quad\text{with }\mathbf{a}_i=\frac{\partial \mathbf{F}_i}{\partial \mathbf{U}} \tag{15.2.27}$$

in which we may use the Roe's average,

$$\mathbf{F}_i=\frac{1}{2}[\mathbf{F}_{ir}+\mathbf{F}_{is}-|\mathbf{a}_i|(\mathbf{U}_r-\mathbf{U}_s)] \tag{15.2.28}$$

as given by (6.2.67).

Implicit time stepping is constructed as

$$\Delta\mathbf{U}^{n+1}=\frac{\Delta t}{\Delta\Omega}\sum\frac{1}{2}\left[\mathbf{F}_{ir}^n+\mathbf{F}_{is}^n-|\mathbf{a}_i|\left(\mathbf{U}_r^n-\mathbf{U}_s\right)\right]n_i\Delta\Gamma \tag{15.2.29}$$

Linearizing, we get

$$\left(\mathbf{I}+\frac{\Delta t}{2\Delta\Omega}\sum|\mathbf{a}_i^*|n_i\Delta\Gamma\right)\Delta\mathbf{U}^{n+1}=\frac{\Delta t}{2\Delta\Omega}\sum\left[\mathbf{F}_{ir}^n+\mathbf{F}_{is}^*-|\mathbf{a}_i^*|\left(\mathbf{U}_r^*-\mathbf{U}_s^n\right)\right]n_i\Delta\Gamma \tag{15.2.30}$$

Here the linearization is performed with an iterative solution in mind, and the asterisk indicates that the term is evaluated using the latest available solution in an adjacent element. Then the iterative procedure may be regarded as a point Gauss-Seidel method requiring the inversion of a 4×4 matrix for each element in the computational grid.

(b) Viscous Contributions. The inviscid equation (15.2.31) may be modified to include the viscous contributions. Noting that

$$\int_\Gamma \mathbf{G}_i^{n+1}n_i d\Gamma=\int_\Gamma\left(\mathbf{G}_i^n+\Delta\mathbf{G}_i\right)n_i d\Gamma$$

or

$$\sum\mathbf{G}_i^{n+1}n_i d\Gamma=\sum\left(\mathbf{G}_i^n+\mathbf{b}_i\Delta\mathbf{U}\right)n_i d\Gamma \tag{15.2.31}$$

Substituting (15.2.32) into (15.2.26) through (15.2.31) we obtain

$$\left[\mathbf{I}+\frac{\Delta t}{\Delta\Omega}\sum\left(\frac{1}{2}|\mathbf{a}_i^*|-\mathbf{b}_i\right)n_i\Delta\Gamma\right]\Delta\mathbf{U}^{n+1}$$
$$=-\frac{\Delta t}{\Delta\Omega}\sum\left\{\frac{1}{2}\left[\mathbf{F}_{ir}^n+\mathbf{F}_{is}^*-|\mathbf{a}_i^*|\left(\mathbf{U}_r^*-\mathbf{U}_s^n\right)\right]-\mathbf{G}_i^*\right\}n_i\Delta\Gamma \tag{15.2.32}$$

The Galerkin approximation of (15.2.30 or 15.2.32) with the upwinded finite element equations in the finite volume formulation leads to

$$(A_{\alpha\beta}\delta_{rs} + B_{\alpha\beta rs})\Delta \mathbf{U}_{\beta s} = W_{\alpha r} \tag{15.2.33}$$

Here the diffusion terms are calculated along the control surfaces similarly as the convection terms.

(4) FVM with FDV

The FDV concept introduced in Sections 6.5 and 13.6 can be used for FVM formulations. To this end, we begin with the FDV governing equations,

$$\mathbf{R} = \left(\mathbf{I} + \mathbf{E}_i^n \frac{\partial}{\partial x_i} + \mathbf{E}_{ij}^n \frac{\partial^2}{\partial x_i \partial x_j}\right)\Delta \mathbf{U}^{n+1} + \mathbf{Q}^n \tag{15.2.34}$$

The FVM integration equation is of the form

$$\int_\Omega \mathbf{R}\, d\Omega = \int_\Omega \left[\left(\mathbf{I} + \mathbf{E}_i^n \frac{\partial}{\partial x_i} + \mathbf{E}_{ij}^n \frac{\partial^2}{\partial x_i \partial x_j}\right)\Delta \mathbf{U}^{n+1} + \mathbf{Q}^n\right] d\Omega = 0 \tag{15.2.35}$$

Integrating (15.2.35) with respect to the spatial coordinates, we obtain

$$\int_\Omega \Delta \mathbf{U}^{n+1}\, d\Omega + \int_\Gamma \left(\mathbf{E}_i \Delta \mathbf{U}^{n+1} + \mathbf{E}_{ij} \Delta \mathbf{U}_{,j}^{n+1}\right) n_i\, d\Gamma = -\int_\Omega \mathbf{Q}^n\, d\Omega \tag{15.2.36}$$

or

$$\sum_{CV} \Delta \mathbf{U}^{n+1}\, \Delta\Omega + \sum_{CS} \left(\mathbf{E}_i \Delta \mathbf{U}^{n+1} + \mathbf{E}_{ij} \Delta \mathbf{U}_{,j}^{n+1}\right) n_i\, \Delta\Gamma = -\int_\Omega \mathbf{Q}^n\, d\Omega \tag{15.2.37}$$

where

$$\int_\Omega \mathbf{Q}^n\, d\Omega = \int_\Gamma \left(\mathbf{H}_i^n + \mathbf{H}_{ij,j}^n\right) n_i\, d\Gamma = \sum_{CS} \left(\mathbf{H}_i^n + \mathbf{H}_{ij,j}^n\right) n_i\, \Delta\Gamma \tag{15.2.38}$$

with

$$\mathbf{H}_i^n = \Delta t\left(\mathbf{F}_i^n + \mathbf{G}_i^n\right), \quad \mathbf{H}_{ij}^n = \frac{\Delta t^2}{2}(\mathbf{a}_i + \mathbf{b}_i)\left(\mathbf{F}_j^n + \mathbf{G}_j^n\right) \tag{15.2.39a,b}$$

15.2.3 THREE-DIMENSIONAL PROBLEMS

Three-dimensional geometries may be discretized using hexahedral elements or tetrahedral elements. Determination of direction cosines for the subcontrol surfaces, subcontrol surface areas, and subcontrol volumes follows the same procedures for FVM via FDM. Formulations and solutions of FVM equations via FEM for three-dimensional problems are carried out similarly as in the two-dimensional case which has been detailed in Section 15.2.

Although hexahedral elements are easy for implementation in general, we may use tetrahedrals with each volume subdivided internally into four volumes corresponding to each vertexs, as shown in Figure 15.2.5a. Within a single tetrahedral, each node shares a common face with each of the neighboring nodes within the tetrahedral. The Green-Gauss theorem is applied to the sub-volume surrounding each vertex to equate the change in mass, momentum, and energy to the convective and diffusive fluxes passing

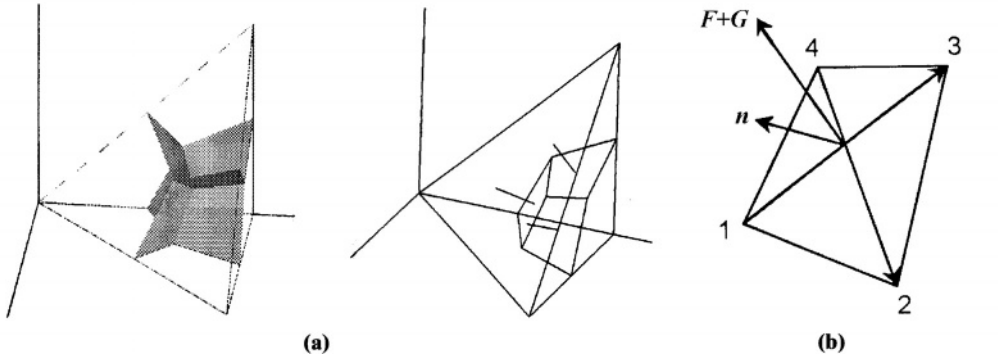

Figure 15.2.5 Tetrahedral element discretization and control volume representation **(a)** Tetrahedral element discretization **(b)** Flux through tetrahedral control volume.

through the control volume faces. Surface normals for each face are obtained via a cross-product as shown in Figure 15.2.5b. Finite element shape functions are used to interpolate the convective and diffusive fluxes at the center of each face.

An overall balance is obtained for a given nodal point by summing the contributions from all of the tetrahedral subvolumes within the mesh that happen to contain the given nodal point. (The nodal control volume is the sum of all of the subvolumes from the tetrahedrals that contain the node.) Note that the fluxes between adjacent tetrahedral volumes cancel since the flux is contained within a single nodal control volume, while identical fluxes through tetrahedral surfaces exposed on the external boundary do not.

15.3 EXAMPLE PROBLEMS

(1) Two-Dimensional Euler Equations, Scramjet Flame Holder Problem

Given:

$$\frac{\partial \mathbf{U}}{\partial t} + \frac{\partial \mathbf{F}_i}{\partial x_i} = 0$$

Inlet Boundary Conditions:

$$\gamma = 1.4, \qquad R = 1716\frac{\text{ft}^2}{\text{s}^2{}^\circ\text{R}} = 287\frac{\text{m}^2}{\text{s}^2{}^\circ\text{K}}$$

$$M = 2, \qquad \rho = 0.002378\frac{\text{slugs}}{\text{ft}^3} = 1.2215\frac{\text{kg}}{\text{m}^3}$$

$$\text{v} = 0, \qquad p = 2116\frac{\text{lbf}}{\text{ft}^2} = 101314.08\,\text{Pa}$$

Outlet Boundary Conditions. Supersonic outflow

Initial Conditions. Use inlet boundary conditions as initial conditions for all nodes.

Required: Use FVM via FEM using two step TGM.

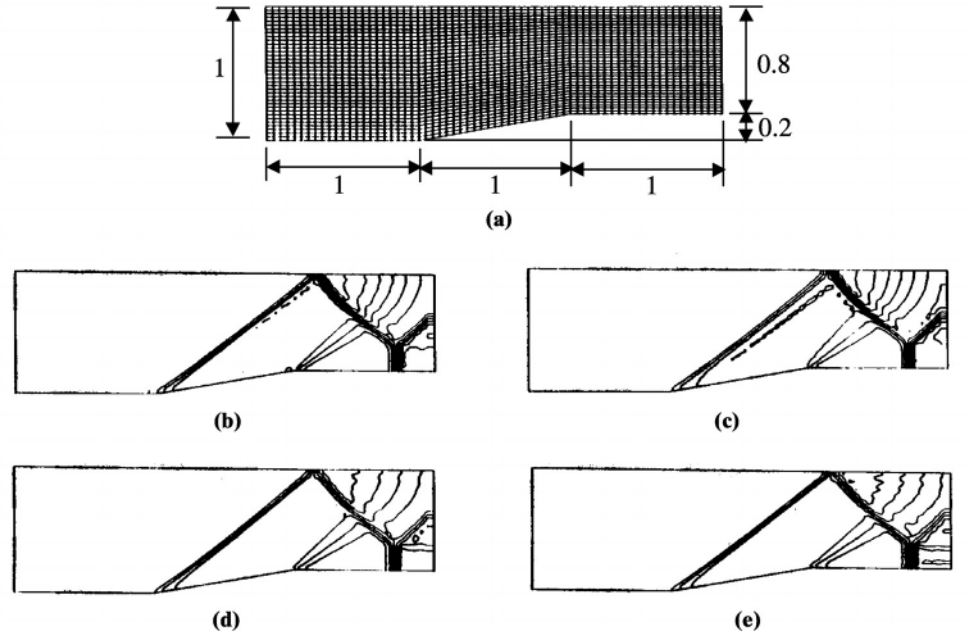

Figure 15.3.1 Solution of Euler equation by FVM-FEM. **(a)** Geometry and discretization. **(b)** Density contours. **(c)** Pressure. **(d)** Temperature contours. **(e)** Mach number contours.

Solution Procedure: The two steps given by (15.2.23) and 15.2.24) will be followed. Here the diffusion terms are zero and the details of the evaluation of convection terms along the control surfaces are calculated as follows:

Step 1

$$\mathbf{U}^{n+\frac{1}{2}} = \mathbf{U}^n - \frac{\Delta t}{2}\left(\frac{\partial \mathbf{F}_x^n}{\partial x} + \frac{\partial \mathbf{F}_y^n}{\partial y}\right)$$

or

$$\begin{aligned}\mathbf{U}_e^{n+\frac{1}{2}} &= \mathbf{U}_e^n - \frac{\Delta t}{2}\sum_{CS}\left(\mathbf{F}_x^n n_1 + \mathbf{F}_y^n n_2\right)\frac{\Delta\Gamma}{\Delta\Omega_e} \\ &= \frac{1}{4}\left(\mathbf{U}_1^n + \mathbf{U}_2^n + \mathbf{U}_3^n + \mathbf{U}_4^n\right) \\ &\quad - \frac{\Delta t}{4}\left\{\left[\left(\mathbf{F}_{x1}^n + \mathbf{F}_{x2}^n\right)n_1 + \left(\mathbf{F}_{y1}^n + \mathbf{F}_{y2}^n\right)n_2\right]\Delta\Gamma_1\right. \\ &\quad + \left[\left(\mathbf{F}_{x2}^n + \mathbf{F}_{x3}^n\right)n_1 + \left(\mathbf{F}_{y2}^n + \mathbf{F}_{y3}^n\right)n_2\right]\Delta\Gamma_2 \\ &\quad + \left[\left(\mathbf{F}_{x3}^n + \mathbf{F}_{x4}^n\right)n_1 + \left(\mathbf{F}_{y3}^n + \mathbf{F}_{y4}^n\right)n_2\right]\Delta\Gamma_3 \\ &\quad \left. + \left[\left(\mathbf{F}_{x4}^n + \mathbf{F}_{x1}^n\right)n_1 + \left(\mathbf{F}_{y4}^n + \mathbf{F}_{y1}^n\right)n_2\right]\Delta\Gamma_4\right\}\Big/\Delta\Omega_e\end{aligned}$$

Step 2

$$\mathbf{U}^{n+1} = \mathbf{U}^n - \frac{\Delta t}{2}\left(\frac{\partial \mathbf{F}_x^{n+\frac{1}{2}}}{\partial x} + \frac{\partial \mathbf{F}_y^{n+\frac{1}{2}}}{\partial y}\right)$$

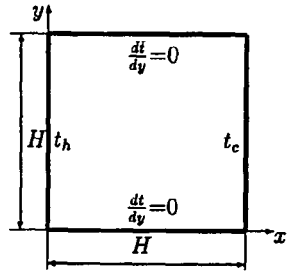

(a)

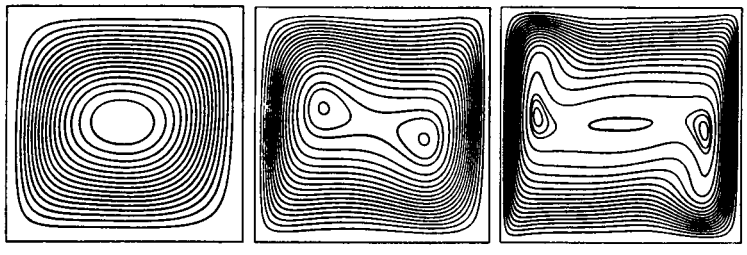

Ra=10^4 Ra=10^5 Ra=10^6

(b)

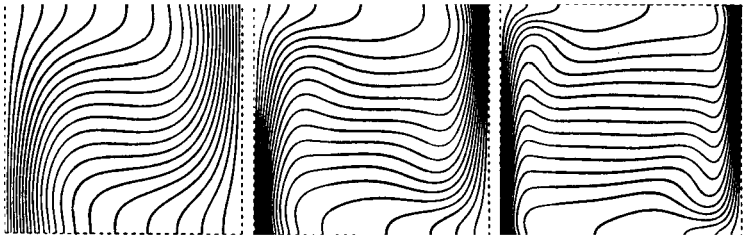

Ra=10^4 Ra=10^5 Ra=10^6

(c)

Figure 15.3.2 Free convection in cavity solution by FVM with FEM [Darbandi and Schneider, 1999]. **(a)** Geometry. **(b)** Streamlines in the cavity, grid 80 × 80. **(c)** Isotherms in the cavity, grid 80 × 80.

or

$$\begin{aligned}\mathbf{U}_e^{n+1} = \mathbf{U}_e^n - \frac{\Delta t}{2}\Big\{&\Big[\Big(\mathbf{F}_{xe1}^{n+\frac{1}{2}} + \mathbf{F}_{xe2}^{n}\Big)n_1 + \Big(\mathbf{F}_{ye1}^{n+\frac{1}{2}} + \mathbf{F}_{ye2}^{n+\frac{1}{2}}\Big)n_2\Big]\Delta\Gamma_1 \\ &+ \Big[\Big(\mathbf{F}_{xe2}^{n+\frac{1}{2}} + \mathbf{F}_{xe3}^{n+\frac{1}{2}}\Big)n_1 + \Big(\mathbf{F}_{ye2}^{n+\frac{1}{2}} + \mathbf{F}_{ye3}^{n+\frac{1}{2}}\Big)n_2\Big]\Delta\Gamma_2 \\ &+ \Big[\Big(\mathbf{F}_{xe3}^{n+\frac{1}{2}} + \mathbf{F}_{xe4}^{n+\frac{1}{2}}\Big)n_1 + \Big(\mathbf{F}_{ye3}^{n+\frac{1}{2}} + \mathbf{F}_{ye4}^{n+\frac{1}{2}}\Big)n_2\Big]\Delta\Gamma_3 \\ &+ \Big[\Big(\mathbf{F}_{xe4}^{n+\frac{1}{2}} + \mathbf{F}_{xe1}^{n+\frac{1}{2}}\Big)n_1 + \Big(\mathbf{F}_{ye4}^{n+\frac{1}{2}} + \mathbf{F}_{ye1}^{n+\frac{1}{2}}\Big)n_2\Big]\Delta\Gamma_4\Big\}\Big/\Delta\Omega_e\end{aligned}$$

The above procedure was carried out, using the geometry and discretization (2479 nodes) as shown in Figure 15.3.1a. It is seen that shock waves develop at the compression corner and expansion waves at the expansion corner as expected. This work is a part of

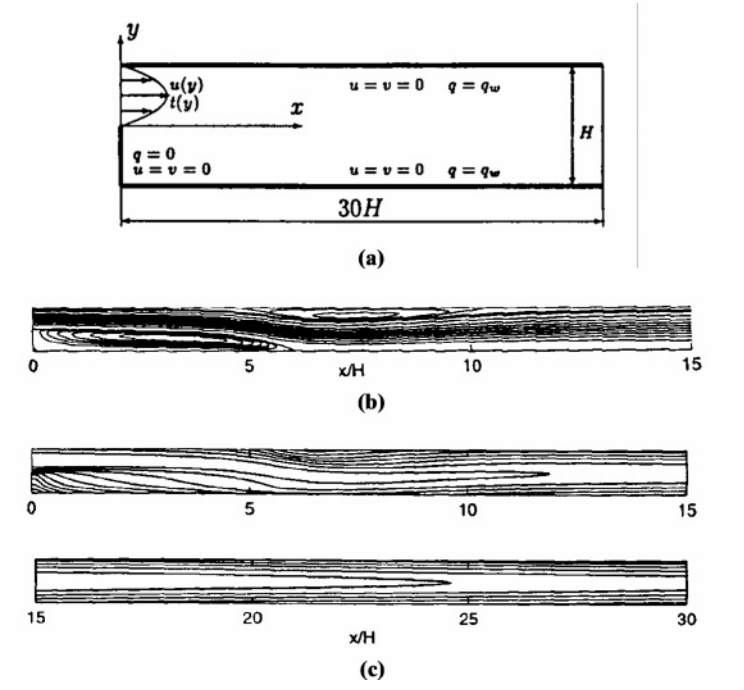

Figure 15.3.3 Backward facing step with forced convection, solution by FVM with FEM [Darbandi and Schneider, 1999.] **(a)** Schematic illustration of the backward facing step problem. **(b)** Stream function contours within the first half of the domain, grid 80 × 20. **(c)** Isotherms in the first (top) and second (bottom) halves of the domain.

the homework assignments in one of the CFD classes at the University of Alabama in Huntsville.

(2) Free Convection in a Cavity

This example is based on the article by Darbandi and Schneider [1999] in which the finite volume method with fully implicit FEM scheme is used to solve the Navier-Stokes system of equations. Here, the source terms with the Rayleigh number for gravity are also included.

In Figure 15.3.2a, the convecting cavity flow geometry and boundary conditions are shown. Computations using 80×80 grid are carried out for Rayleigh numbers of $Ra = 10^4, 10^5$, and 10^6. The corresponding results are shown in Figure 15.3.2b and 15.3.2c for the isotherms and streamlines, respectively. Effects of Rayleigh numbers are clearly shown, with distorted distributions being more prominent for higher Rayleigh numbers. Further details are found in Darbandi and Schneider [1999].

(3) Backward Facing Step with Forced Convection

Another example reported by the same authors above is the backward facing step with forced convection (Figure 15.3.3a). Solutions using 80×20 grid show stream function contours and isotherms in Figures 15.3.3b and 15.3.3c, respectively. The advantages of using FVM with FEM have been demonstrated in this work with further details found in Darbandi and Schneider [1999].

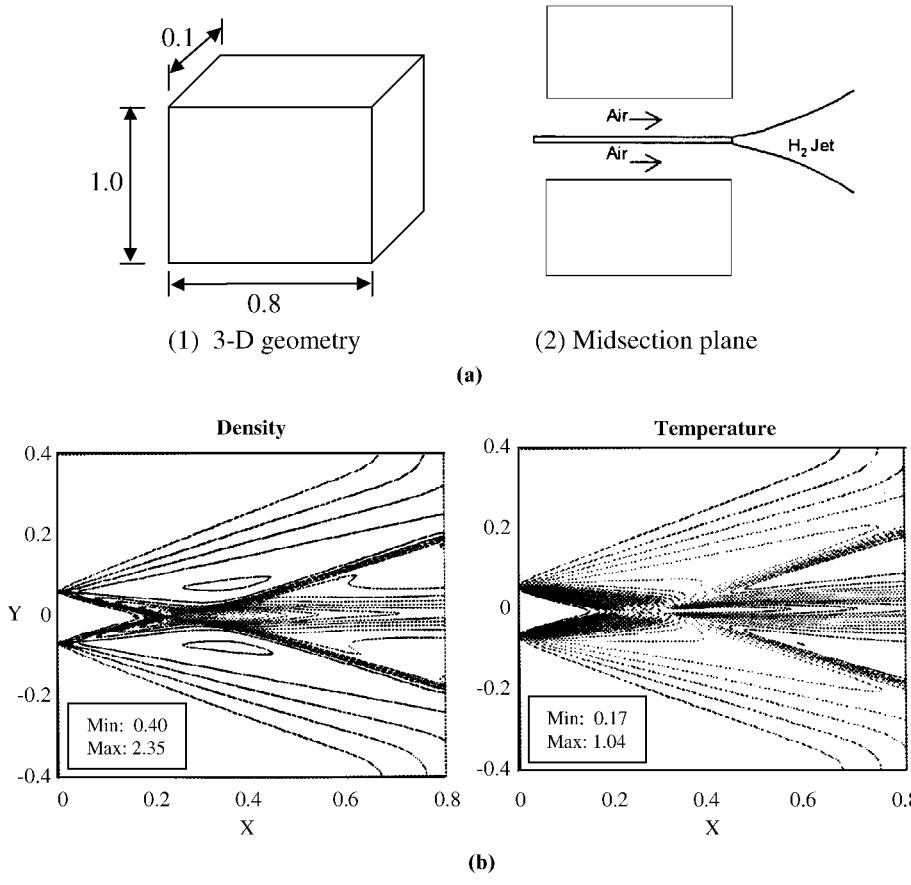

Figure 15.3.4 Density and temperature distributions, supersonic hydrogen-air injection flow analysis using finite volume tetrahedral elements (nonreacting case) with FVM-FDM-FDV [Schunk and Chung, 2000]. **(a)** Analysis by FVM with tetrahedral elements of Figure 15.2.5. **(b)** Density and temperature contours for nonreacting flowfield.

(4) Three-Dimensional Supersonic Propulsion Injection Flows

This is an example to demonstrate the use of three-dimensional tetrahedral elements with FVM-FE-FDV as shown in Figure 15.2.5 [Schunk and Chung, 2000]. Pure hydrogen is injected into a Mach 1.9 airstream at 1495 K (Figure 15.3.4a). The hydrogen is injected at Mach 2.0 and 251 K. Hydrogen is preburned in the air stream to produce a flow that contains 28% water along with 48% hydrogen and 24% oxygen. The static pressure of both the jet and the airstream is 1 atmosphere.

Steady-state density and temperature contours are shown in Figure 15.3.4b for the nonreacting flow case. It is shown that expansion waves are formed as the air flow is turned into and mixes with the hydrogen jet. Downstream, oblique shocks are formed as the main flow is turned back parallel with the free stream.

15.4 SUMMARY

In this chapter, we have shown that the finite volume methods can be formulated using FEM. This is the counterpart of Chapter 7 where the FDM was used to formulate

FVM. Although many practitioners use finite volume methods formulated from FDM or FEM, critical comparisons between the two methods have not been pursued. As has been the case from the beginning, the purpose of this text is to encourage the reader to learn all available approaches. It is hoped that in this manner, our knowledge in CFD will be enhanced to a greater extent in the future.

Most of the computational methods in CFD using FDM and FEM have been discussed. Undoubtedly, there are some topics that should have been included. Instead, our intention is to come to an end at this point, review what we have discussed so far, and seek comparisons and relationships between FDM and FEM. Moreover, there are computational methods other than FDM, FEM, and FVM. These and other topics will be presented in the next chapter.

REFERENCES

Darbandi, M. and Schneider, G. E. [1999]. Application of an all-speed flow algorithm to heat transfer problems. *Num. Heat Trans.*, 35, 695–715.

Masson, C., Saabas, H. J., and Baliga, B. R. [1994]. Co-located equal order control volume finite element method for two-dimensional axisymmetric incompressible fluid flow. *Int. J. Num. Meth. Eng.*, 18, 12–26.

Schneider, G. E. and Raw, M. J. [1987]. Control volume finite element method for heat transfer and fluid flow using colocated variables – 1. Computational procedure. *Num. Heat Trans.*, 11, 363–399.

Schunk, R. G. and Chung, T. J. [2000]. Airbreathing propulsion system analysis using multithreaded parallel processing. AIAA paper, AIAA-2000-3467.